Research Article | Vol. 30, No. 2 / 17 Jan 2022 / Optics Express 2792
Optics EXPRESS

Generation of entanglement between a highly wave-packet-tunable photon and a spin-wave memory in cold atoms

YA LI,[1,2] YAFEI WEN,[1,2,3] SHENGZHI WANG,[1,2] CHAO LIU,[1,2] HAILONG LIU,[1,2] MINJIE WANG,[1,2] CAN SUN,[1,2] YAN GAO,[1,2] SHUJING LI,[1,2,4] AND HAI WANG[1,2,5]

[1]*The State Key Laboratory of Quantum Optics and Quantum Optics Devices, Institute of Opto-Electronics, Shanxi University, Taiyuan 030006, China*
[2]*Collaborative Innovation Center of Extreme Optics, Shanxi University, Taiyuan 030006, China*
[3]*Department of Physics, Taiyuan Normal University, Jinzhong 030619, China*
[4]*lishujing@sxu.du.cn*
[5]*wanghai@sxu.edu.cn*

Abstract: Controls of waveforms (pulse durations) of single photons are important tasks for effectively interconnecting disparate atomic memories in hybrid quantum networks. So far, the waveform control of a single photon that is entangled with an atomic memory remains unexplored. Here, we demonstrated control of waveform length of the photon that is entangled with an atomic spin-wave memory by varying light-atom interaction time in cold atoms. The Bell parameter S as a function of the duration of photon pulse is measured, which shows that violations of Bell inequality can be achieved for the photon pulse in the duration range from 40 ns to 50 μs, where, $S = 2.64 \pm 0.02$ and $S = 2.26 \pm 0.05$ for the 40-ns and 50-μs durations, respectively. The measured results show that S parameter decreases with the increase in the pulse duration. We confirm that the increase in photon noise probability per pulse with the pulse-duration is responsible for the S decrease.

1. Introduction

Quantum networks (QWs) play an important role in distributed long-distance quantum communications [1–3] and quantum computations [4,5]. The quantum interfaces that generate entanglement between an atomic memory and a photon [6–16] can be used as quantum node and then are basic building blocks for QWs. The elementary step in QWs is to establish entanglement between two remote memories (nodes) [1–2]. With the quantum interfaces, one can establish entanglement between two remote memories by performing two-photon Hong-Ou-Mandel interference [17–22]. Also, the remote-memory entanglement can be established by mapping quantum state of a photon entangled with an atomic memory into another remote memory [23]. Hybrid quantum networks use disparate quantum memory (QM) systems as nodes and then can benefit from the advantages of the disparate systems. In hybrid QWs, an open question is wave-packet matching of the interfacing photons that are generated from or stored in disparate memory matters (nodes). For example, the pulse widths of the single photons generated from disparate memory matters are different. Specifically, the typical pulse widths of single photons are ~3 ns [24] for single quantum dots, ~0.4 [25,26] μs for solid-state atomic ensemble, ~70-100 ns [8,9,12] for cold atoms, 1 ns [27] (40 μs [28]) for room-temperature atomic vapors via off-resonance (motional averaging) Duan–Lukin–Cirac–Zoller protocol, and ~0.5 μs [23] or 12 μs [29] for single atoms or ions in QED cavities. Also, for achieving high-efficiency optical quantum storages in different memory matters via various storage schemes, the required pulse-widths of the single photons are different. For example, the required pulse-width is 200ns-3μs for

#446837 https://doi.org/10.1364/OE.446837
Journal © 2022 Received 26 Oct 2021; revised 11 Dec 2021; accepted 5 Jan 2022; published 12 Jan 2022

Optics EXPRESS

cold atoms [30–34] via EIT storage scheme, ~7 μs for crystals [35] via AFC storage scheme, 0.7μs for single atom via EIT storage scheme [36], 1 ns for hot atoms [37], 7 ns for cold atoms [38] and ~260 fs for bulk diamond [39] via Raman storage scheme, respectively. However, HOM interference requires that the wave-packets of the two photons are perfectly overlapped, if not, visibility of HOM dip will be degraded [40]. So, the perfect wave-packet matching of the two photons is necessary for establishing hybrid QWs. Recently, two experiments have experimentally demonstrated the non-classical correlation between two different memories [41], and HOM interferometer between two photons from two different memory matters [42], where the wave-packets of the single photons are changed into appropriate values, and then the connection between the different memories are experimentally available. With various physical systems such as cavity-quantum-electrodynamics single atom [43], a single trapped ion [44], DLCZ quantum memory in cold atomic ensemble [45], cold atoms [46–49] and hot atomic vapour [50] with four-wave-mixing, the single photons with highly tunable waveform lengths have been experimentally demonstrated. However, in these experiments the single photon is only non-classically correlated with or stored in an atomic memory, it is not entangled with an atomic memory. Thus, the influences of changes of single-photon wave-packet on the atom-photon entanglement remain unexplored.

In this article, we demonstrated controls of temporal durations of waveform of the Stokes photon entangled with an atomic spin-wave memory in cold atoms via varying DLCZ-like light-atom interaction time. The retrieval efficiency R and Bell parameter S as a function of the width of Stokes-photon pulse are measured. The results show that in the width ranging from 40 ns to 50 μs, the retrieval efficiency is basically kept unchanged and the violation of the Bell inequality can be achieved. Specifically, when the pulse width is 40 ns, we achieved R= 20% and S= 2.64 ± 0.02, while when it is 50 μs, we achieved R= 15% and S= 2.26 ± 0.05, respectively. To our knowledge, the 50 μs long wave packet of a single photon represents the longest wave packet of a single photon entangled with an atomic spin-wave memory. By fitting the experimental data with theoretical calculations, we reveal the reason for the decrease in S parameter with the pulse duration, which results from that background noise per pulse increases with the pulse duration.

2. Experimental setup

The experimental setup is shown in Fig. 1(a). The atomic ensemble is a cloud of cold ^{87}Rb atoms, whose relevant atomic levels are shown in Fig. 1(b), where, $|g\rangle = |5^2S_{1/2}, F = 1\rangle$, $|s\rangle = |5^2S_{1/2}, F = 2\rangle$, $|e_1\rangle = |5^2P_{1/2}, F' = 1\rangle$, and $|e_2\rangle = |5^2P_{1/2}, F' = 2\rangle$. Each level includes Zeeman sublevels, for example, $|g\rangle$ is written as $|g, m\rangle$, where the magnetic quantum number $m = \pm 1, 0$. After the atoms are released from the magneto-optical trap, we prepare the atoms into Zeeman levels $|g, m = \pm 1,0\rangle$ via optical pumping with a cleaning laser. In the beginning of a spin-wave-photon entanglement (SWPE) generation trial [Fig. 1(c)], a write laser pulse with a tunable duration τ_w is applied onto the atoms. The value of the duration τ_w is controlled by an AOM (see Fig. 1(a)). The write pulse is Δ=20 MHz blue-detuned to $|g\rangle \rightarrow |e_2\rangle$ transition, which induces spontaneous Raman scattering of σ^--polarized (σ^+-polarized) Stokes photons and simultaneously create the spin wave $|+\rangle(|-\rangle)$, where the spin wave $|+\rangle(|-\rangle)$ is associated with the coherence $|g, m = 0\rangle \leftrightarrow |s, m = 0\rangle$ and $|g, m = -1\rangle \leftrightarrow |s, m = -1\rangle$ ($|g, m = -1\rangle \leftrightarrow |s, m = 1\rangle$ and $|g, m = 0\rangle \leftrightarrow |s, m = 2\rangle$), which is shown in Fig. 1(b). Also, the spin coherence $|g, m = -1\rangle \leftrightarrow |s, m = -1\rangle$ will be created in the spontaneous Raman scattering, but is neglected in the spin wave $|+\rangle$ since it can't be retrieved in the following retrieval step. In the Stokes detection channel (purple dash line in Fig. 1(a)), we transform the $\sigma^+(\sigma^-)$-polarized Stokes photons into the horizontally- (H-) or vertically- (V-) polarized photon by a λ/4 plate. The joint state of the atom–photon system may be written as [7,51] $\rho_{ap} = |0\rangle\langle 0| + \sqrt{\chi}|\Phi_{\text{a - p}}\rangle\langle\Phi_{\text{a - p}}|$, where $|0\rangle$ denotes the vacuum, $\chi(\ll 1)$ represents the probability of creating the $|\Phi_{\text{a - p}}\rangle$ state per write pulse, $\Phi_{\text{a - p}} = (\cos\vartheta|+\rangle_a|H\rangle_S + \sin\vartheta|-\rangle_a|V\rangle_S)$ denotes the spin-wave-photon entanglement

Optics EXPRESS

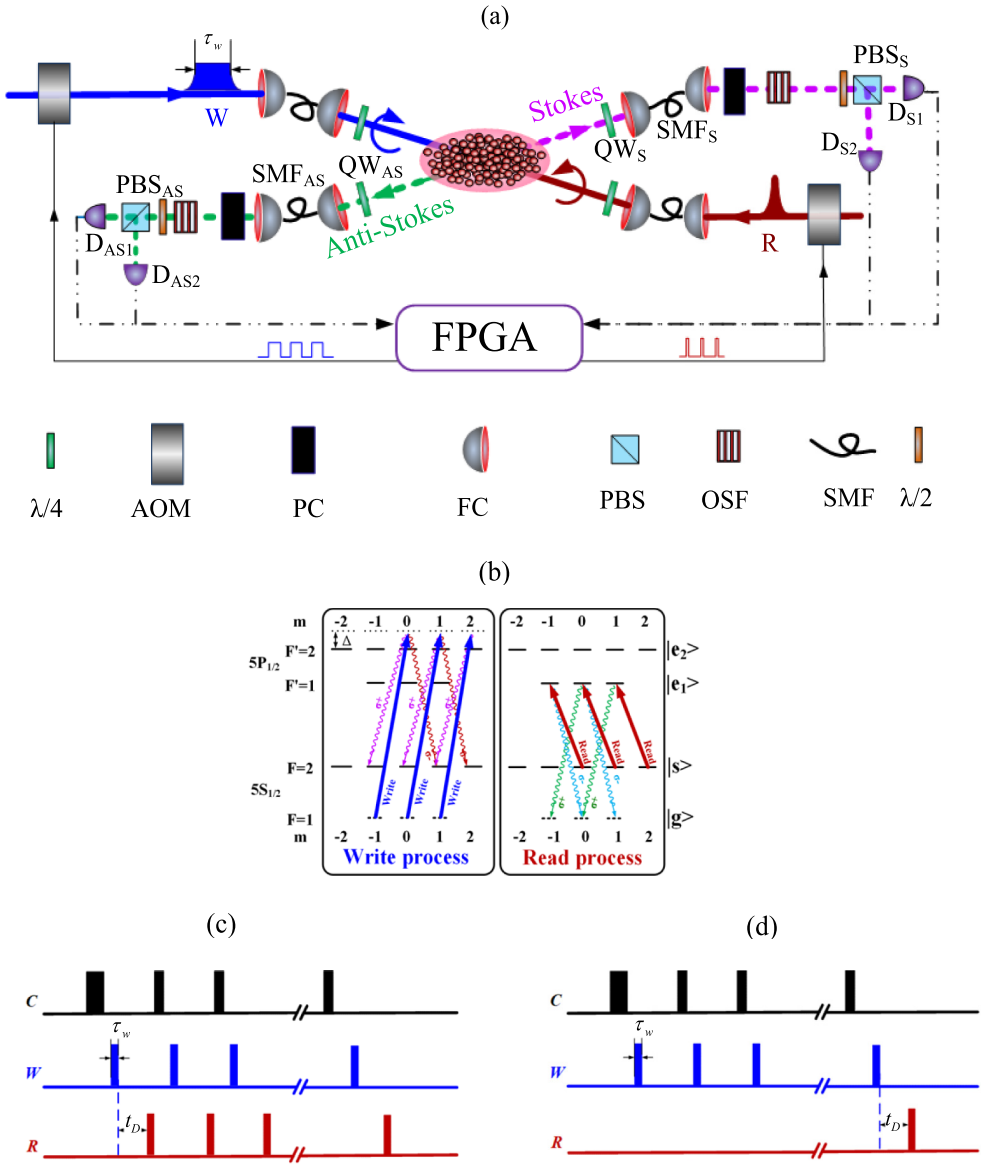

Fig. 1. Overview of the experiment. (a) Experimental setup. $\lambda/4(\lambda/2)$ quarter-wave (half-wave) plate; AOM: acousto-optic modulator; PC: phase compensation module; FC: fiber collimator; PBS: polarizing beam splitter; OSFS: optical-spectrum-filter set; SMF: Single-mode fiber; D_{S1}, D_{S2}, D_{AS1}, D_{AS2}: Single photon detectors (SPCM-NIR, Excelitas Technologies); FPGA: programmable gate array; (b) Relevant atomic levels. ↻ (↺) represents σ^-−−(σ^+) –polarized write (read) laser beam; (c) Time sequence of the experimental trials for measuring the Bell parameter S ; (d) Time sequence of the experimental trials for measuring cross-correlation function $g_{S,AS}$ and retrieval efficiency . W, C, R: write, cleaning and read laser pulses (all the lasers are DL Pro made in TOPTICA Photonics), t_D denotes the time delay between the write and read pulses.

Optics EXPRESS

state, $|H\rangle_S$ ($|V\rangle_S$) denotes a H- (V-) polarized Stokes photon, $\cos\vartheta$ is the relevant Clebsch-Gordan coefficient with the asymmetric angle of $\vartheta \approx 0.81 * (\pi/4)$[6]. The Stokes photons are collected at about 1°relative to the direction of the write laser beam (blue line), which defines their wave vector $\boldsymbol{k_S}$. The collection is achieved by a single-mode fiber, which is labeled as $\mathrm{SMF_S}$ in Fig. 1(a). The wave-vector of the spin-wave excitation is given by $\boldsymbol{k_{SWE}} = \boldsymbol{k_W} - \boldsymbol{k_S}$, where, $\boldsymbol{k_W}$ is the wave-vector of the write pulse. After the SMF_S, the Stokes photons go through a phase compensator (PC) [52], which is used to eliminate the phase shift between the H and V polarizations caused by SMF_S. Next, the Stokes photons pass through an optical-spectrum-filter set (OSFS) which consists of three Fabry-Perot etalons. Blocking by OSFS, the leakage of the write laser beam in the Stokes channel was attenuated by a factor of 10^{-9}. We then measured the background noise probability resulting from the write laser beam in the Stokes channel, which is not more than 2.5×10^{-4}/write pulse in our presented experiment. The OSFS transmit the Stokes field with a transmission efficiency of ~70%. Subsequently, the Stokes photon passes through a $\lambda/2$ plate. By rotating it, one can change the polarization angle θ_S of the Stokes fields. Then, the Stokes photon is guided to a polarizing beam splitter PBS_S, which transmits the horizontal (H) polarization to a detector D_{S1} and reflects the vertical (V) polarization to a detector D_{S2} for $\theta_S = 0$. The detection events at the detectors D_{S1} and D_{S2} are analyzed with a field programmable gate array (FPGA). As soon as a Stokes photon is detected by D_{S1} or D_{S2}, the storage of a spin-wave in $|+\rangle$ or $|-\rangle$ mode is herald. Thus, the FPGA will send out a feed-forward signal to stop the write process. After a time delay t_D, a σ^--polarized read laser pulse that is resonant on the $|s\rangle \rightarrow |e_1\rangle$ transition and counter-propagates with the write beam is applied to convert the spin wave $|+\rangle$ ($|-\rangle$) into a $\sigma^-(\sigma^+)$ -polarized anti-Stokes photon. According to the phase-matching condition $\boldsymbol{k_W} - \boldsymbol{k_S} = \boldsymbol{k_{AS}} - \boldsymbol{k_R}$, where $\boldsymbol{k_R}$ is the wave vector of the read laser pulse, the retrieved (anti-Stokes) photon directs into the spatial mode determined by the wave-vector $\boldsymbol{k_{AS}} \approx -k_S$, i.e., it propagates in the opposite direction to the Stokes photon. The $\sigma^-(\sigma^+)$ -polarized anti-Stokes fields are transformed into H (V) -polarized field by a $\lambda/4$ plate labelled as $\mathrm{QW_{AS}}$ in Fig. 1(a). Thus, the atom–photon state $\Phi_{\mathrm{a-p}}$ is transformed into the two-photon entangled state $\Phi_{\mathrm{pp}} = \cos\vartheta|H\rangle_S|H\rangle_{AS} + \sin\vartheta|V\rangle_S|V\rangle_{AS}$, where, $|H\rangle_{AS}$ ($|V\rangle_{AS}$) denotes a H- (V-) polarized anti-Stokes (readout) photon. As shown in Fig. 1(a), the channel for collecting and detecting anti-Stokes (readout) photon is similar to that for the Stokes (write-out) photon. The two outputs of $\mathrm{PBS_{AS}}$ are sent to single-photon detectors D_{AS1} (D_{AS2}). The polarization angle θ_{AS} of the anti-Stokes field is changed by rotating a $\lambda/2$ plate before $\mathrm{PBS_{AS}}$. After the retrieval, a cleaning pulse with a duration of 200 ns is applied to pump the atoms into the initial level $|g\rangle$. Then, the next trial starts. If no Stokes photon is detected during the write process, the atoms will be directly pumped back into the initial level by the read and cleaning pulses. Subsequently the next trial starts. The time sequence of the above-mentioned SWPE is shown in Fig. 1(c). While, in the measurement for the cross-correlation function $g_{S,AS}$ which is defined in the following Eq. (5), we will apply a write pulse following by a cleaning laser pulse and then apply a read pulse. Such cycle is repeated by a large number in the measurement. The time sequence of the measurement for $g_{S,AS}$ is shown in Fig. 1(d).

3. Experimental results

By changing the write-laser pulse duration τ_w, we varied the atom-light interaction time and then demonstrated the control of Stokes-photon wave-packet length. With the increase in the write-pulse duration τ_w, we decreased write laser power and fixed the Stokes excitation probability at $\chi \approx 1\%$ in this demonstration. The Stokes photon counts C_S are measured according to $C_S = C_{D_{S1}} + C_{D_{S2}}$, where $C_{D_{S1}}(C_{D_{S2}})$ is the photon counts at D_{S1} (D_{S2}) for the polarization angle $\theta_S = 0$. Figure 2(a), (b) and (c) show the three examples of the measured Stokes-photon histograms when the widths of the write pulses are $\tau_w = 40\ ns$, $\tau_w = 5\ \mu s$ and $\tau_w = 50\ \mu s$. The red lines in these figures are the temporal wave shapes of the Stokes photon without any background

Optics EXPRESS

subtraction. The blue lines represent background noise levels. The wave-shape durations of the Stokes-photon in (a), (b) and (c) are ~40ns, ~5 μs and ~50 μs, respectively, which show that the durations τ_S of the Stokes-photon pulses are the same as that of the applied write-laser pulses, i.e., $\tau_S \approx \tau_w$. It should be pointed out that since the background noise probability resulting from the write laser is not more than 2.5×10^{-4}/write pulse, it doesn't influence on the fixing of the excitation probability 1%.

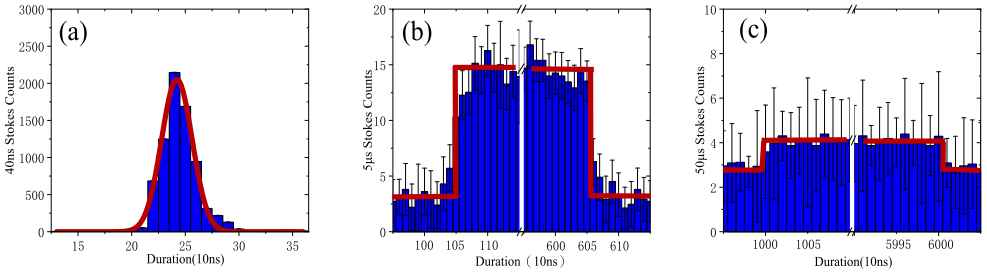

Fig. 2. Three examples of the Stokes-photon temporal wave shapes. The Stokes photons are generated by applying write pulses with (a) 40 ns, (b) 5μs and (c) 50μs durations (full-width at half-maximum, FWHM). All detection events were binned into 10 ns.

The quantum correlations between the Stokes and anti-Stokes photons can be characterized by the cross-correlation function

$$g_{S,AS} = P_{S,AS}/(P_S P_{AS}) \tag{1}$$

where, $P_{S,AS}$ is the coincident detection probability between the Stokes and anti-Stokes photons, $P_S(P_{AS})$ denotes the probability of detecting one Stokes (anti-Stokes) photon. In our presented experiment, the coincident detection probability $P_{S,AS}$ is measured as $P_{S,AS} = P_{D_{S1},D_{AS1}} + P_{D_{S2},D_{AS2}} + P_{D_{S2},D_{AS1}} + P_{D_{S1},D_{AS2}}$ for the polarization angles $\theta_S = \theta_{AS} = 0$, where, for example, $P_{D_{S1},D_{AS1}}$ ($P_{D_{S2},D_{AS1}}$) is the probability of detecting a coincidence between the detectors D_{S1} and D_{AS1}(D_{S2} and D_{AS1}). $P_S(P_{AS})$ is measured as $P_S = P_{D_{S1}} + P_{D_{S2}}(P_{AS} = P_{D_{AS1}} + P_{D_{AS2}})$, where, for example, $P_{D_{S1}}$ ($P_{D_{AS2}}$) is the probability of detecting a photon at D_{S1} (D_{AS2}). In the measurements of $P_{S,AS}$, the polarization angles are set to be $\theta_S = \theta_{AS} = 0$.

The Stokes, anti-Stokes and coincidence detection probabilities can be expressed as:

$$P_S = \chi\eta_S + B\eta_S \tag{2}$$

$$P_{AS} = \chi\gamma\eta_{AS} + (1-\gamma)\xi\eta_{AS} + C\eta_{AS} \tag{3}$$

$$P_{S,AS} = \chi\gamma\eta_S\eta_{AS} + P_S P_{AS} \tag{4}$$

respectively, where, B (C) denotes background noise probability per Stokes (anti-Stokes) pulse in the Stokes (anti-Stokes) channel, η_{AS} (η_S) is the overall detection efficiencies in the channel, whose values are $\eta_{AS} \approx \eta_S \approx 0.3$ in the presented experiment, γ is the retrieval efficiency, the second term in Eq. (4) represent the noise resulting from imperfect readout [53], ξ is the branching ratio corresponding to the read photon transition [53].

We then measured the background noise probability B per Stokes-photon (write-laser) pulse when the duration of the write pulse is changed from 40 ns to 50 μs. Since the duration of the Stokes pulse τ_S equal to that of the write-pulse duration τ_w, we set the detection time interval of the Stokes photon to be equal to τ_w. The background noise probability B includes the dark counts of single-photon detectors, leakages of the laser beams in the experimental system due to imperfect switch off, as well as the photon counts from the write-laser leakage. It doesn't include the emission from the atoms. So, we measured it without the trapped atoms. When measuring the background noise probability, the write laser power was decreased with increasing the write-pulse

Optics EXPRESS

duration. For each duration value, by setting the write laser power to an appropriate value, the excitation probability was fixed at $\chi \approx 1\%$, which is the same as the measurement in Fig. 2. The measured results are shown in Fig. 3. We find that the noise probability B increases linearly with the width τ_w, i.e., it can be written as $B = k\tau_w$ with $k = 4.84 \times 10^{-4}/1\mu s$.

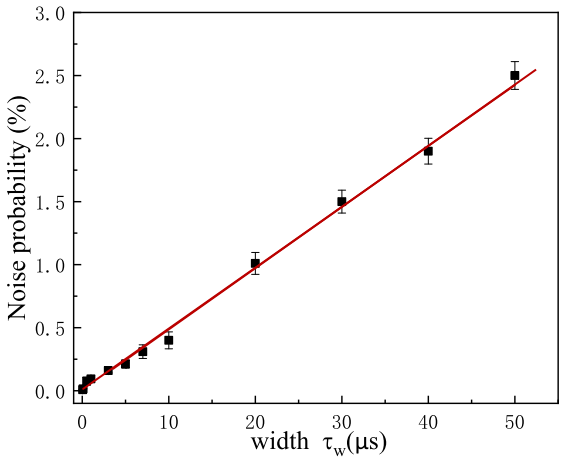

Fig. 3. The measured background noise probability B as a function of the width τ_w. The fitting (red line) to the experimental data is based on $B = k\tau_w$ with $k = 4.84 \times 10^{-4}/1\mu s$.

The retrieval efficiency is measured as $\gamma \approx (P_{S,AS} - P_S P_{AS})/[\eta_{AS} \cdot (P_S - B\eta_S)]$. The time sequence of measurement for the retrieval efficiency is the same as that for $g_{S,AS}$ in Fig. 1(d). Figure 4(a) plots the measured retrieval efficiency as a function of time delay t_D of the read laser pulse for the case that 100 ns write pulse is applied, where the time interval for detecting Stokes photon is set to be 100 ns. In this measurement since the write-pulse duration τ_w is very small, the time delay t_D corresponds to the storage time t, i.e., $t \approx t_D$. From Fig. 4(a), one can see that the measured retrieval efficiency decreases with the increase in storage time t due to spin-wave decoherence. The solid (blue) line in Fig. 4(a) is the fitting to the measured data according to $\gamma(t) \approx \gamma_0 e^{-(t/\tau_0)^2}$ with $\gamma_0 = 22\%$, which yields a memory lifetime of $\tau_0 \approx 53\mu s$. Figure 4(b) plots the measured retrieval efficiency as a function of the width τ_w for a fixed storage time t of ~1μs, where the time interval for detecting Stokes photon is set to be the width of τ_w. As shown in Fig. 4(b), the measured retrieval efficiencies decrease with the increase in the width τ_w. The main physical reason for this decrease explained below. Actually, when the write pulse with duration τ_w is applied onto the atoms, the spin wave may be generated at any time during the range of $[t_D,\ t_D + \tau_w/2]$. So, the average storage time of the spin wave can be written as $t = t_D + \tau_w/2$. For the case that $\tau_w \approx \tau_0$, for example, $\tau_w \approx 50\mu s$, the average spin-wave storage time in Fib.4(b) is $t = t_D + \tau_w/2 \approx 26\mu s$. After such an average storage time, the decoherence of the spin wave will be distinctly, which will lead to a significant decrease in the retrieval efficiency. Such a decrease can be evaluated according to the measured result in Fig. 4(a), where the retrieval efficiency will decrease by 22% after a storage time of 26μs. So, the spin-wave decay with increasing storage time t is a main reason for that the retrieval efficiency decreases with the excitation pulse duration τ_w. Another physical reason for the decrease in Fig. 4(b) probably results from the spin-wave decay with increasing the interaction time between the write-laser pulse and the atoms. Driving by the weak write-laser pulse, the atoms, which are initially prepared in the state $|5S_{1/2}, F = 1\rangle$, will be excited to the state $|5P_{1/2}, F' = 2\rangle$ with a small probability of $P_e \sim (\Omega_w \tau_w)^2$ [53,54], where, Ω_w denotes the Rabi frequency of the write-laser beam. The population in the excited state will decay to $|5S_{1/2}, F = 1\rangle$ via spontaneous emissions, which will induce atomic random motion and then lead to a spin-wave decay with increasing the duration τ_w. Due to such spin-wave decay,

Optics EXPRESS

the retrieval efficiency decreases with the duration τ_w. To precisely understand the relationship between the retrieval efficiency and the excitation pulse duration, and the possible decoherence factor, further studies are needed.

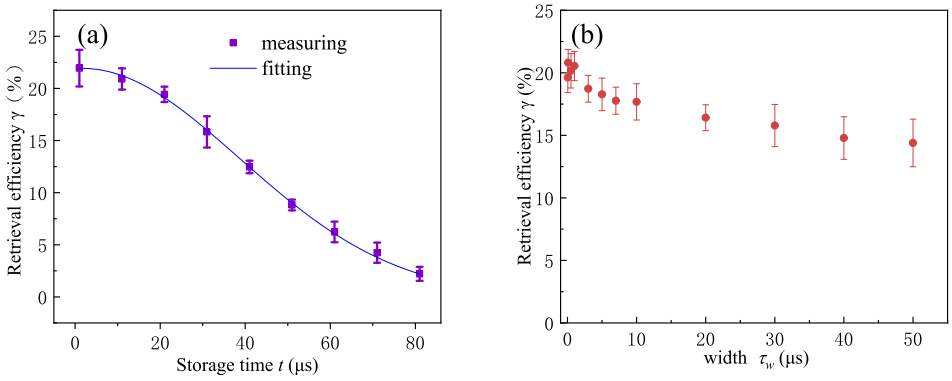

Fig. 4. (a) Measured retrieval efficiency γ as a function of storage time t (temporal delay between the read and write laser pulses), where the write-pulse duration is set to a fixed value of $\tau_w = 100ns$. (b) Measured retrieval efficiency γ as a function of write-pulse width τ_w, where the time delay is set to a fixed value t_D=1μs. In both measurements, the excitation probability is set to the fixed value $\chi \approx 1\%$.

According to the Eq. (1), we measured the cross-correlation function $g_{S,AS}$ as a function of the width τ_w for a fixed excitation probability $\chi \approx 1\%$ per trial (write pulse) and the time delay between the read and write pulses $t_D = 1\mu s$. In the measurement, the time interval for detecting Stokes photon is set to be τ_w . As shown in Fig. 5, the value of $g_{S,AS}$ decrease with the increase in the width τ_w. We attribute such decrease to the increase in the background noise B and the decrease in the retrieval efficiency γ with the width τ_w. This view point can be explained by the following theoretical calculations. According to the expressions of $P_{S,AS}$, P_S and P_{AS}, we rewrite the quantum correlation $g_{S,AS}$ as:

$$\begin{aligned} g_{S,AS} = P_{S,AS}/(P_S P_{AS}) &= 1 + \frac{\gamma(\tau_w)}{(B+\chi)\gamma(\tau_w) + (B+\chi)(1-\gamma(\tau_w))\xi + C + BC/\chi} \\ &= 1 + \frac{\gamma(\tau_w)}{(k\tau_w+\chi)\gamma(\tau_w) + (k\tau_w+\chi)(1-\gamma(\tau_w))\xi + C + k\tau_w C/\chi} \end{aligned} \tag{5}$$

where, $B = k\tau_w$, which is given in Fig. 3, has been put into the Eq. (5), $\gamma(\tau_w)$ is the retrieval efficiency as a function of the width τ_w, whose values can be obtained from the measured data shown in Fig. 4(b). The black solid curve in Fig. 5 is the fitting to the experimental data based on the Eq. (5) with the experimental parameters including the excitation probability $\chi \approx 1\%$ and the temporal delay t_D=1μs. Also, the branching ratio is set to be $\xi = 0.27$ in the fitting. One can see that the fitting is in agreement with the experimental data $g_{S,AS}$.

The quality of the spin-wave-photon entanglement can be described by the Clauser–Horne–Shimony–Holt Bell parameter S, which is written as:

$$S = |E(\theta_S, \theta_{AS}) - E(\theta_S, \theta'_{AS}) + E(\theta'_S, \theta_{AS}) + E(\theta'_S, \theta'_{AS})| < 2$$

with the correlation function $E(\theta_S, \theta_{AS})$ defined by:

$$\frac{C_{D_{S_1},D_{AS_1}}(\theta_S,\theta_{AS}) + C_{D_{S_2},D_{AS_2}}(\theta_S,\theta_{AS}) - C_{D_{S_1},D_{AS_2}}(\theta_S,\theta_{AS}) - C_{D_{S_2},D_{AS_1}}(\theta_S,\theta_{AS})}{C_{D_{S_1},D_{AS_1}}(\theta_S,\theta_{AS}) + C_{D_{S_2},D_{AS_2}}(\theta_S,\theta_{AS}) + C_{D_{S_1},D_{AS_2}}(\theta_S,\theta_{AS}) + C_{D_{S_2},D_{AS_1}}(\theta_S,\theta_{AS})} \tag{6}$$

Optics EXPRESS

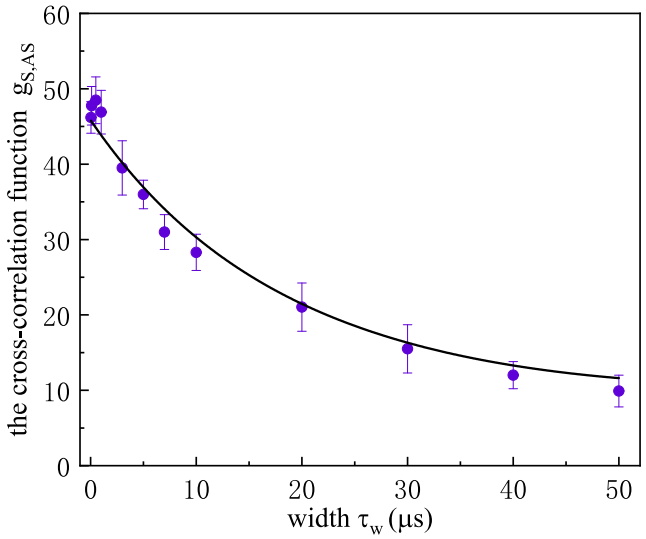

Fig. 5. The measured cross-correlation function $g_{S,AS}$ as a function of the width τ_w. In the measurement, the time interval for detecting Stokes photon is set to be the corresponding value of τ_w. The black solid curve is the fitting to the measured data based on Eq. (5) with the experimental parameters of $\chi \approx 1\%$ and t_D=1μs. In the fitting, the branching ratio is set to be $\xi = 0.27$.

where, for example, $C_{D_{S1},D_{AS1}}(\theta_S, \theta_{AS})$ ($C_{D_{S_2},D_{AS_2}}(\theta_S, \theta_{AS})$) denotes the coincidence counts between detectors D_{S1} (D_{S2}) and D_{AS1} (D_{AS2}) for the polarization angles θ_S and θ_{AS}. In the S measurement, we used the canonical settings $\theta_S = 0°$, $\theta'_S = 45°$, $\theta_{AS} = 22.5°$, and $\theta'_{AS} = 67.5°$. To demonstrate how the changes of wave-packet length of the Stokes photon does influences the atom-photon entanglement quality, we measured Bell parameter S as a function of the width τ_w for $\chi = 1\%$ and show the measured data in Fig. 6. In the measurement, the time interval for detecting Stokes photon is set to be τ_w. One can see that the values of S decrease with the increase in the width τ_w. At $\tau_w = 40ns$, $S = 2.64 \pm 0.02$, which violates the CHSH inequality by 32 standard deviations. At $\tau_w = 50\mu s$, $S = 2.26 \pm 0.05$, which violates the CHSH inequality by 5 standard deviations. The dependence of the Bell parameter on the write-pulse width τ_w can be written as :

$$S(\tau_w) = 2\sqrt{2}V_0\frac{g_{S,AS}(\tau_w) - 1}{g_{S,AS}(\tau_w) + 1} \tag{7}$$

where, V_0 is the initial visibility ($\tau_w = 100ns$), which is $V_0 \approx 95.7\%$ in the presented experiment and is main limited to the imperfect phase compensation of the optical elements and the asymmetry angle ϑ. Based on the Eq. (7), we plot the fitting (red solid curve) to the experimental data of S in Fig. 6, where the values of $g_{S,AS}(\tau_w)$ are obtained from the data in Fig. 5. One can see that the fitting is in agreement with the experimental data S, showing that the reduction of S as the width τ_w has the same reason, i.e., the reduction of S results from the increase in the background noise B and the decrease in the retrieval efficiency with the width τ_w.

Optics EXPRESS

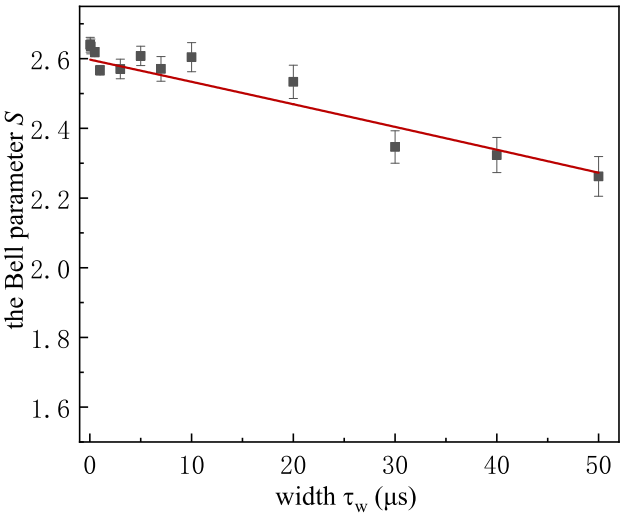

Fig. 6. The measured Bell parameter S as a function of the width τ_w. The red solid curve is the fitting to the measured data based on Eq. (7) with the parameter $V_0 \approx 95.7\%$ and the values of $g_{S,\mathrm{AS}}(\tau_w)$ taken from the data in Fig. 5.

4. Conclusion

Based on atom-photon entanglement generation via DLCZ scheme, we demonstrated the control of waveform length of the Stokes photon by varying light-atom interaction time in cold atoms. The Bell parameter S as the function of the duration of the Stokes photon pulse (write-pulse width) is measured, which shows that violations of the Bell inequality can be achieved for the Stokes photon pulse in the duration ranging from 40 ns to 50 μs with S= 2.64±0.02 and S= 2.26±0.05 for 40 ns and 50 μs durations, respectively. To our knowledge, the 50 μs long wave packet of a single photon represents the longest wave packet of single photon non-classically correlated with or entangled with an atomic spin-wave memory. In the next works, the bandwidth of the Stokes-photon should be measured, which is important quantity in Hong-Ou-Mandel interference [55]. Another question in hybrid QWs is the wavelength matching of the interfacing photons from two disparate atomic memories. By using cascaded quantum frequency conversion [41], one can overcome this question. In our presented experiment, the dark state in the readout, which is mentioned in the experimental setup, leads to a loss in the retrieval efficiency. In the next works, different energy level without any dark states should be selected and then the loss in the retrieval efficiency will be avoided. In summary, our presented work provides a road to achieve entanglement between a single photon with highly tunable wave shape and a spin-wave memory and then benefits for hybrid quantum networks.

Funding. Ministry of Science and Technology of the People's Republic of China (2016YFA0301402); National Natural Science Foundation of China (12174235); Fund for Shanxi Key Subjects Construction (1331).

Disclosures. The authors declare no conflicts of interest.

Data availability. Data underlying the results presented in this paper are not publicly available at this time but may be obtained from the authors upon reasonable request.

References

1. N. Sangouard, C. Simon, H. de Riedmatten, and N. Gisin, "Quantum repeaters based on atomic ensembles and linear optics," Rev. Mod. Phys. **83**(1), 33–80 (2011).
2. L.-M. Duan, M. D. Lukin, J. I. Cirac, and P. Zoller, "Long-distance quantum communication with atomic ensembles and linear optics," Nature **414**(6862), 413–418 (2001).
3. C. Simon, "Towards a global quantum network," Nat. Photonics **11**(11), 678–680 (2017).

Optics EXPRESS

4. H. J. Kimble, "The quantum internet," Nature **453**(7198), 1023–1030 (2008).
5. A. Reiserer and G. Rempe, "Cavity-based quantum networks with single atoms and optical photons," Rev. Mod. Phys. **87**(4), 1379–1418 (2015).
6. D. N. Matsukevich, T. Chaneliere, M. Bhattacharya, S. Y. Lan, S. D. Jenkins, T. A. Kennedy, and A. Kuzmich, "Entanglement of a photon and a collective atomic excitation," Phys. Rev. Lett. **95**(4), 040405 (2005).
7. H. de Riedmatten, J. Laurat, C. W. Chou, E. W. Schomburg, D. Felinto, and H. J. Kimble, "Direct measurement of decoherence for entanglement between a photon and stored atomic excitation," Phys. Rev. Lett. **97**(11), 113603 (2006).
8. S. Chen, Y. A. Chen, B. Zhao, Z. S. Yuan, J. Schmiedmayer, and J. W. Pan, "Demonstration of a stable atom-photon entanglement source for quantum repeaters," Phys. Rev. Lett. **99**(18), 180505 (2007).
9. S. J. Yang, X. J. Wang, J. R. J. Li, X. H. Bao, and J. W. Pan, "Highly Retrievable Spin-Wave-Photon Entanglement Source," Phys. Rev. Lett. **114**(21), 210501 (2015).
10. Y. O. Dudin, A. G. Radnaev, R. Zhao, J. Z. Blumoff, T. A. Kennedy, and A. Kuzmich, "Entanglement of light-shift compensated atomic spin waves with telecom light," Phys. Rev. Lett. **105**(26), 260502 (2010).
11. X. J. Wang, S. J. Yang, P. F. Sun, B. Jing, J. Li, M. T. Zhou, X. H. Bao, and J. W. Pan, "Cavity-Enhanced Atom-Photon Entanglement with Subsecond Lifetime," Phys. Rev. Lett. **126**(9), 090501 (2021).
12. S.-Z. Wang, M.-J. Wang, Y.-F. Wen, Z.-X. Xu, T.-F. Ma, S.-J. Li, and H. Wang, "Long-lived and multiplexed atom-photon entanglement interface with feed-forwardcontrolled readouts," Commun. Phys. **4**(1), 168 (2021).
13. R. Ikuta, T. Kobayashi, T. Kawakami, S. Miki, M. Yabuno, T. Yamashita, H. Terai, M. Koashi, T. Mukai, T. Yamamoto, and N. Imoto, "Polarization insensitive frequency conversion for an atom-photon entanglement distribution via a telecom network," Nat. Commun. **9**(1), 1997 (2018).
14. W. Chang, C. Li, Y. K. Wu, N. Jiang, S. Zhang, Y. F. Pu, X. Y. Chang, and L. M. Duan, "Long-Distance Entanglement between a Multiplexed Quantum Memory and a Telecom Photon," Phys. Rev. X **9**(4), 041033 (2019).
15. E. Saglamyurek, N. Sinclair, J. Jin, J. A. Slater, D. Oblak, F. Bussieres, M. George, R. Ricken, W. Sohler, and W. Tittel, "Broadband waveguide quantum memory for entangled photons," Nature **469**(7331), 512–515 (2011).
16. C. Clausen, I. Usmani, F. Bussieres, N. Sangouard, M. Afzelius, H. de Riedmatten, and N. Gisin, "Quantum storage of photonic entanglement in a crystal," Nature **469**(7331), 508–511 (2011).
17. B. Zhao, Z. B. Chen, Y. A. Chen, J. Schmiedmayer, and J. W. Pan, "Robust creation of entanglement between remote memory qubits," Phys. Rev. Lett. **98**(24), 240502 (2007).
18. Z. S. Yuan, Y. A. Chen, B. Zhao, S. Chen, J. Schmiedmayer, and J. W. Pan, "Experimental demonstration of a BDCZ quantum repeater node," Nature **454**(7208), 1098–1101 (2008).
19. Y. Yu, F. Ma, X. Y. Luo, B. Jing, P. F. Sun, R. Z. Fang, C. W. Yang, H. Liu, M. Y. Zheng, X. P. Xie, W. J. Zhang, L. X. You, Z. Wang, T. Y. Chen, Q. Zhang, X. H. Bao, and J. W. Pan, "Entanglement of two quantum memories via fibres over dozens of kilometres," Nature **578**(7794), 240–245 (2020).
20. X. Liu, J. Hu, Z. F. Li, X. Li, P. Y. Li, P. J. Liang, Z. Q. Zhou, C. F. Li, and G. C. Guo, "Heralded entanglement distribution between two absorptive quantum memories," Nature **594**(7861), 41–45 (2021).
21. D. Lago-Rivera, S. Grandi, J. V. Rakonjac, A. Seri, and H. de Riedmatten, "Telecom-heralded entanglement between multimode solid-state quantum memories," Nature **594**(7861), 37–40 (2021).
22. J. Hofmann, M. Krug, N. Ortegel, L. Gerard, M. Weber, W. Rosenfeld, and H. Weinfurter, "Heralded entanglement between widely separated atoms," Science **337**(6090), 72–75 (2012).
23. S. Ritter, C. Nolleke, C. Hahn, A. Reiserer, A. Neuzner, M. Uphoff, M. Mucke, E. Figueroa, J. Bochmann, and G. Rempe, "An elementary quantum network of single atoms in optical cavities," Nature **484**(7393), 195–200 (2012).
24. Y.-M. He, Y. He, Y.-J. Wei, D. Wu, M. Atatu, C. Schneider, M. K. Sven Ho, C.-Y. Lu, and J.-W. Pan, "On-demand semiconductor single-photon source with near-unity indistinguishability," Nat. Nanotechnol. **8**(3), 213–217 (2013).
25. C. Laplane, P. Jobez, J. Etesse, N. Gisin, and M. Afzelius, "Multimode and Long-Lived Quantum Correlations Between Photons and Spins in a Crystal," Phys. Rev. Lett. **118**(21), 210501 (2017).
26. K. Kutluer, M. Mazzera, and H. de Riedmatten, "Solid-State Source of Nonclassical Photon Pairs with Embedded Multimode Quantum Memory," Phys. Rev. Lett. **118**(21), 210502 (2017).
27. J.-P. Dou, A.-L. Yang, M.-Y. Du, D. Lao, J. Gao, L.-F. Qiao, H. Li, X.-L. Pang, Z. Feng, H. Tang, and X.-M. Jin, "A broadband DLCZ quantum memory in room-temperature atoms," Commun. Phys. **1**(1), 55 (2018).
28. K. B. Dideriksen, R. Schmieg, M. Zugenmaier, and E. S. Polzik, "Room-temperature single-photon source with near-millisecond built-in memory," Nat. Commun. **12**(1), 3699 (2021).
29. A. Stute, B. Casabone, B. Brandstatter, K. Friebe, T. E. Northup, and R. Blatt, "Quantum-state transfer from an ion to a photon," Nat. Photonics **7**(3), 219–222 (2013).
30. S.-C. Zhang, S.-Y. Zhou, M. M. T. Loy, G. K. L. Wong, and S.-W. Du, "Optical storage with electromagnetically induced transparency in a dense cold atomic ensemble," Opt. Lett. **36**(23), 4530–4532 (2011).
31. Y.-H. Chen, M.-J. Lee, I.-C. Wang, S.-W. Du, Y.-F. Chen, Y.-C. Chen, and I. A. Yu, "Coherent Optical Memory with High Storage Efficiency and Large Fractional Delay," Phys. Rev. Lett. **110**(8), 083601 (2013).
32. Y.-F. Hsiao, P.-J. Tsai, H.-S. Chen, S.-X. Lin, C.-C. Hung, C.-H. Lee, Y.-H. Chen, Y.-F. Chen, I.-A. Yu, and Y.-C. Chen, "Highly Efficient Coherent Optical Memory Based on Electromagnetically Induced Transparency," Phys. Rev. Lett. **120**(18), 183602 (2018).
33. P. Vernaz-Gris, K. Huang, M. Cao, A. S. Sheremet, and J. Laurat, "Highly-efficient quantum memory for polarization qubits in a spatially-multiplexed cold atomic ensemble," Nat. Commun. **9**(1), 363 (2018).

Optics EXPRESS

34. Y. Wang, J. Li, S. Zhang, K. Su, Y. Zhou, K. Liao, S. Du, H. Yan, and S.-L. Zhu, "Efficient quantum memory for single-photon polarization qubits," Nat. Photonics **13**(5), 346–351 (2019).
35. A. Holzäpfel, J. Etesse, K. Kaczmarek, A. Tiranov, N. Gisin, and M. Afzelius, "Optical storage for 0.53 s in a solid-state atomic frequency comb memory using dynamical decoupling," New J. Phys. **22**(6), 063009 (2020).
36. K. F. Reim, J. Nunn, V. O. Lorenz, B. J. Sussman, K. C. Lee, N. K. Langford, D. Jaksch, and I. A. Walmsley, "Towards high-speed optical quantum memories," Nat. Photonics **4**(4), 218–221 (2010).
37. H. P. Specht, C. Nolleke, A. Reiserer, M. Uphoff, E. Figueroa, S. Ritter, and G. Rempe, "A single-atom quantum memory," Nature **473**(7346), 190–193 (2011).
38. D.-S. Ding, W. Zhang, Z.-Y. Zhou, S. Shi, B.-S. Shi, and G.-C. Guo, "Raman quantum memory of photonic polarized entanglement," Nat. Photonics **9**(5), 332–338 (2015).
39. D. G. England, K. A. Fisher, J. P. MacLean, P. J. Bustard, R. Lausten, K. J. Resch, and B. J. Sussman, "Storage and retrieval of THz-bandwidth single photons using a room-temperature diamond quantum memory," Phys. Rev. Lett. **114**(5), 053602 (2015).
40. Z. S. Yuan, Y. A. Chen, S. Chen, B. Zhao, M. Koch, T. Strassel, Y. Zhao, G. J. Zhu, J. Schmiedmayer, and J. W. Pan, "Synchronized independent narrow-band single photons and efficient generation of photonic entanglement," Phys. Rev. Lett. **98**(18), 180503 (2007).
41. N. Maring, P. Farrera, K. Kutluer, M. Mazzera, G. Heinze, and H. de Riedmatten, "Photonic quantum state transfer between a cold atomic gas and a crystal," Nature **551**(7681), 485–488 (2017).
42. A. N. Craddock, J. Hannegan, D. P. Ornelas-Huerta, J. D. Siverns, A. J. Hachtel, E. A. Goldschmidt, J. V. Porto, Q. Quraishi, and S. L. Rolston, "Quantum Interference between Photons from an Atomic Ensemble and a Remote Atomic Ion," Phys. Rev. Lett. **123**(21), 213601 (2019).
43. O. Morin, M. Korber, S. Langenfeld, and G. Rempe, "Deterministic Shaping and Reshaping of Single-Photon Temporal Wave Functions," Phys. Rev. Lett. **123**(13), 133602 (2019).
44. M. Almendros, J. Huwer, N. Piro, F. Rohde, C. Schuck, M. Hennrich, F. Dubin, and J. Eschner, "Bandwidth-tunable single-photon source in an ion-trap quantum network," Phys. Rev. Lett. **103**(21), 213601 (2009).
45. P. Farrera, G. Heinze, B. Albrecht, M. Ho, M. Chavez, C. Teo, N. Sangouard, and H. de Riedmatten, "Generation of single photons with highly tunable wave shape from a cold atomic ensemble," Nat. Commun. **7**(1), 13556 (2016).
46. S. Du, P. Kolchin, C. Belthangady, G. Y. Yin, and S. E. Harris, "Subnatural linewidth biphotons with controllable temporal length," Phys. Rev. Lett. **100**(18), 183603 (2008).
47. K. Liao, H. Yan, J. He, S. Du, Z. M. Zhang, and S. L. Zhu, "Subnatural-linewidth polarization-entangled photon pairs with controllable temporal length," Phys. Rev. Lett. **112**(24), 243602 (2014).
48. L. Zhao, X. Guo, C. Liu, Y. Sun, M. M. T. Loy, and S. Du, "Photon pairs with coherence time exceeding 1 μs," Optica **1**(2), 84–88 (2014).
49. Z. Han, P. Qian, L. Zhou, J. F. Chen, and W. Zhang, "Coherence time limit of the biphotons generated in a dense cold atom cloud," Sci. Rep. **5**(1), 9126 (2015).
50. C. Shu, P. Chen, T. K. Chow, L. Zhu, Y. Xiao, M. M. Loy, and S. Du, "Subnatural-linewidth biphotons from a Doppler-broadened hot atomic vapour cell," Nat. Commun. **7**(1), 12783 (2016).
51. Y. Wen, P. Zhou, Z. Xu, L. Yuan, H. Zhang, S. Wang, L. Tian, S. Li, and H. Wang, "Multiplexed spin-wave–photon entanglement source using temporal multimode memories and feedforward-controlled readout," Phys. Rev. A **100**(1), 012342 (2019).
52. L. Tian, Z. Xu, L. Chen, W. Ge, H. Yuan, Y. Wen, S. Wang, S. Li, and H. Wang, "Spatial Multiplexing of Atom-Photon Entanglement Sources using Feedforward Control and Switching Networks," Phys. Rev. Lett. **119**(13), 130505 (2017).
53. L. Heller, P. Farrera, G. Heinze, and H. de Riedmatten, "Cold-Atom Temporally Multiplexed Quantum Memory with Cavity-Enhanced Noise Suppression," Phys. Rev. Lett. **124**(21), 210504 (2020).
54. C. J. Foot, "Atomic physics," Oxford (2005).
55. C. K. Hong, Z. Y. Ou, and L. Mandel, "Measurement of subpicosecond time intervals between two photons by interference," Phys. Rev. Lett. **59**(18), 2044–2046 (1987).